BIOCHEMISTRY
including biophysical chemistry & molecular biology

 Volume 48, Number 16 April 28, 2009

*Current Topics*

# A Lysine-Tyrosine Pair Carries Out Acid−Base Chemistry in the Metal Ion-Dependent Pyridine Dinucleotide-Linked β-Hydroxyacid Oxidative Decarboxylases†

Deniz F. Aktas and Paul F. Cook*

*Department of Chemistry and Biochemistry, University of Oklahoma, 620 Parrington Oval, Norman, Oklahoma 73019*

*Received December 16, 2008; Revised Manuscript Received March 11, 2009*

ABSTRACT: This work reviews published structural and kinetic data on the pyridine nucleotide-linked β-hydroxyacid oxidative decarboxylases. The family of metal ion-dependent pyridine nucleotide-linked β-hydroxyacid oxidative decarboxylases can be divided into two structural families with the malic enzyme, which has an (*S*)-hydroxyacid substrate, comprising one subfamily and isocitrate dehydrogenase, isopropylmalate dehydrogenase, homoisocitrate dehydrogenase, and tartrate dehydrogenase, which have an (*R*)-hydroxyacid substrate, comprising the second subclass. Multiple-sequence alignment of the members of the (*R*)-hydroxyacid family indicates a high degree of sequence identity with most of the active site residues conserved. The three-dimensional structures of the members of the (*R*)-hydroxyacid family with structures available superimpose on one another, and the active site structures of the enzymes have a similar overall geometry of residues in the substrate and metal ion binding sites. In addition, a number of residues in the malic enzyme active site are also conserved, and the arrangement of these residues has a similar geometry, although the (*R*)-hydroxyacid and (*S*)-hydroxyacid family sites are geometrically mirror images of one another. The active sites of the (*R*)-hydroxyacid family have a higher positive charge density when compared to those of the (*S*)-hydroxyacid family, largely due to the number of arginine residues in the vicinity of the substrate α-carboxylate and one fewer carboxylate ligand to the divalent metal ion. Data available for all of the enzymes in the family have been considered, and a general mechanism that makes use of a lysine (general base)-tyrosine (general acid) pair is proposed. Differences exist in the mechanism for generating the neutral form of lysine so that it can act as a base.

β-Hydroxyacid oxidative decarboxylation is catalyzed by enzymes that utilize a pyridine dinucleotide, NAD(P). The enzymes included are the well-studied malic enzyme, isocitrate dehydrogenase, and 6-phosphogluconate dehydrogenase, as well as homoisocitrate dehydrogenase, isopropylmalate dehydrogenase, and tartrate dehydrogenase. The β-hydroxyacid oxidative decarboxylases can be classified on the basis of their metal ion dependence. Malic enzyme (*1*−*4*), isocitrate dehydrogenase (*5*−*7*), and isopropylmalate dehydrogenase (*8, 9*) require a divalent metal ion, $Mg^{2+}$ or $Mn^{2+}$, for activity. Homoisocitrate dehydrogenase (*10, 11*) and

† This work was supported by the Grayce B. Kerr Endowment to the University of Oklahoma (to support the research of P.F.C.).

* To whom correspondence should be addressed. E-mail: pcook@ou.edu. Telephone: (405) 325-4581. Fax: (405) 325-7182.

10.1021/bi8022976 CCC: $40.75 
Published on Web 03/12/2009

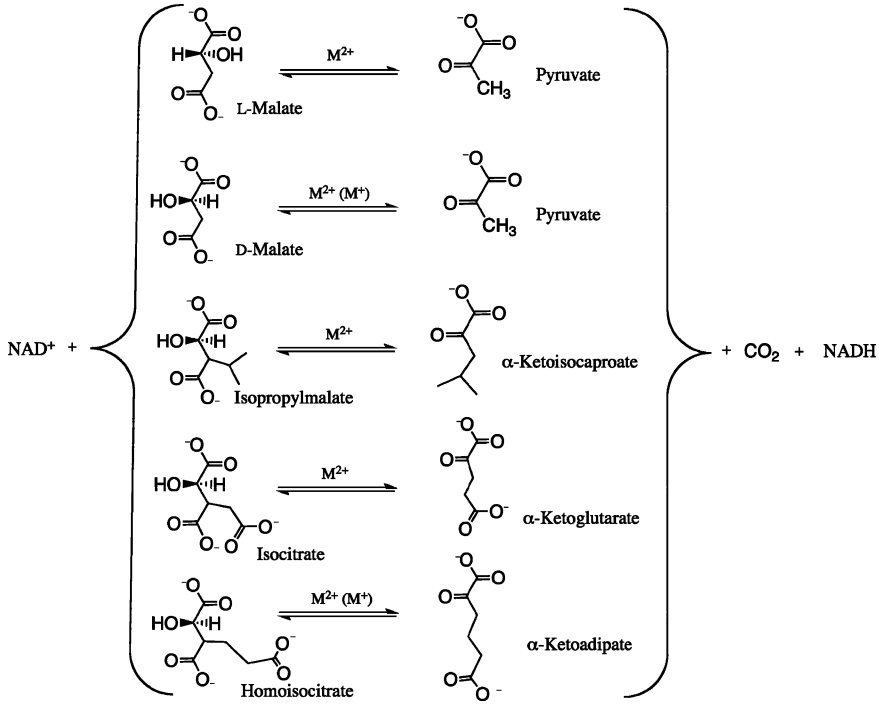


FIGURE 1: Reactions catalyzed by the metal ion-dependent pyridine dinucleotide-linked $\beta$-hydroxyacid oxidative decarboxylases. The dinucleotide substrate and product and $CO_2$ are common to all reactions. The $\beta$-hydroxyacid and ketone product for each of the reactions are shown in parentheses. The metal ion dependencies of each of the enzymes are provided above the arrow. Reactions from top to bottom are catalyzed by malic enzyme, tartrate dehydrogenase, isopropylmalate dehydrogenase, isocitrate dehydrogenase, and homoisocitrate dehydrogenase, respectively.

tartrate dehydrogenase (*12, 13*) require both a monovalent ion (usually $K^+$) and a divalent metal ion for optimal activity. Finally, 6-phosphogluconate dehydrogenase is divalent and monovalent metal ion-independent (*14, 15*). This review will focus on the metal ion-dependent enzymes. In terms of overall structure, the metal ion-dependent enzymes can be divided into two distinct enzyme families. The first includes isocitrate dehydrogenase, isopropylmalate dehydrogenase, homoisocitrate dehydrogenase, and tartrate dehydrogenase, while malic enzyme is in a class of its own.

The reactions catalyzed by the enzymes are listed in Figure 1. Note that the substrates of these enzymes, isocitrate, isopropylmalate, homoisocitrate, and D,L-malate, have a common malate backbone and differ only in the substituent on the carbon $\beta$ to the 1-carboxylate and stereochemistry at C2. The enzymes thus differ in their substrate specificity and are strict in their selection of the substrate for the oxidative decarboxylation reaction [tartrate dehydrogenase catalyzes reactions other than oxidative decarboxylation (*16*)].

In spite of the differences in metal ion requirement and structure, all of the pyridine dinucleotide-linked $\beta$-hydroxyacid oxidative decarboxylases catalyze the same general reaction. The overall reaction proceeds via three steps, oxidation of the $\beta$-hydroxyacid to a $\beta$-ketoacid, decarboxylation to generate an enol, and tautomerization to give a ketone product (Scheme 1).

All the enzymes in the class of metal ion-dependent $\beta$-hydroxyacid oxidative decarboxylases exhibit a steady-state random kinetic mechanism (*16*−*22*). The acid−base chemical mechanisms of some of the enzymes have been proposed, and there are significant differences in the proposed mechanisms (*23*−*29*). In this work, we propose a unified acid−base mechanism for the metal ion-dependent enzymes on the basis of the similarity in the active sites and data presently in the literature. There are a number of reviews that cover aspects other than those considered in this work, and the reader is referred to these for additional information (*30*−*33*).

## STRUCTURE

*Overall Structure.* As suggested in the introductory section, the metal ion-dependent $\beta$-hydroxyacid oxidative decarboxylases apparently fall into two families. An overlay of a dimer of isocitrate dehydrogenase (*27*), isopropylmalate dehydrogenase (*34*), and homoisocitrate dehydrogenase (*35*) is shown in Figure 2A. (No structure is presently available for tartrate dehydrogenase.) There is remarkably good agreement of the backbone structures of all three of the enzymes; they are clearly in the same fold family, which for the sake of convenience we will call the (*R*)-hydroxyacid family. Malic enzyme, on the other hand, neither aligns well nor has a structure similar to those of the other enzymes. In addition, its substrate has the opposite stereochemistry, and we place it in the (*S*)-hydroxyacid family. A superposition of a dimer of the malic enzymes of *Ascaris suum* (*36*), human mitochondria (*37*), and pigeon liver cytosol (*38*) is shown in Figure 2B; the enzyme is tetrameric overall. All are $\alpha\beta$ proteins with a modified Rossmann fold for cofactor binding. The active site is located in the cleft between two subunits for isopropylmalate dehydrogenase, isocitrate dehydrogenase, and homoisocitrate dehydrogenase, while for malic enzyme, the active site is in a cleft with contributions from three domains (*27, 34, 36*). All enzymes adopt a closed conformation of the active site upon substrate binding, via rigid body movement of one domain relative to the other.

Scheme 1: General Mechanism of Pyridine Dinucleotide-Linked, Divalent Metal Ion-Dependent β-Hydroxyacid Oxidative Decarboxylases[a]

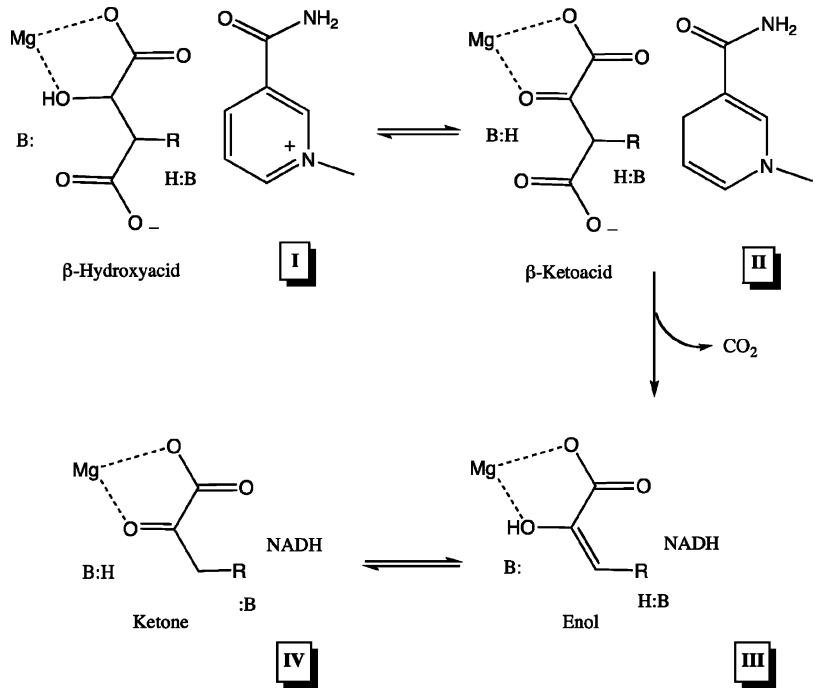


[a] (I) Base-catalyzed oxidation of the β-hydroxyacid to the β-ketoacid. (II) The metal ion acts as a Lewis acid catalyst in the decarboxylation of the β-ketoacid with a general acid assist to give the enol. (III) General acid−base tautomerization of the enol to the ketone product (IV).

A multiple-sequence alignment of the members of the (*R*)-hydroxyacid family is shown in Figure 3. As one can see, active site residues important for reactant and metal ion binding and catalysis are completely conserved in all of the family members. On the other hand, the malic enzymes do not align with the (*R*)-hydroxyacid family members but align with a high degree of identity to one another (Figure 4). Interestingly, alignment of the mitochondrial NAD- and cytosolic NADP-dependent malic enzymes also shows a high (∼50%) level of identity (not shown). The NAD- and NADP-dependent isocitrate dehydrogenases, however, exhibit a low (∼10%) level of identity, but with the active site residues conserved with the exception of one of the arginine residues.

*Active Site.* As expected on the basis of the similarity of the overall structures, the location of the active site within a monomer is the same for all of the enzymes in the (*R*)-hydroxyacid family. Active site residues are contributed by two subunits, with the catalytic lysine and an aspartate metal ligand contributed by one subunit and the remaining residues contributed by the other. The active sites in the (*S*)-hydroxyacid family are completely contained in each of the four subunits of the tetramer.

A close-up view of the active site of the NAD-malic enzyme showing the catalytic residues and those involved in metal ion binding is shown in Figure 5A. The structure is of the dead-end E−$Mn^{2+}$−malate−NADH complex, which is used as a model of the catalytically active E−malate−$Mn^{2+}$−NAD complex. A general acid−general base mechanism and the identities of the catalytic residues have been proposed and will be discussed in Acid−Base Chemical Mechanism. A catalytic triad has been suggested for the *Ascaris* malic enzyme, consisting of a lysine, a tyrosine, and an aspartic acid (*29*). In the substrate-bound form, the metal ion exhibits octahedral coordination, and all of the ligands are oxygens and include three side chain carboxylates, a water molecule, and two substrate functional groups, the α-carboxylate and α-hydroxyl. In addition, the α-carboxylate of malate is further oriented by hydrogen bonding interactions with the side chains of an arginine and two asparagine residues (not shown). The active site of the NADP-malic enzymes is virtually identical to that of the NAD-malic enzymes.

Active site close-ups in stereo of isopropylmalate dehydrogenase, isocitrate dehydrogenase, and homoisocitrate dehydrogenase are shown in panels B−D, respectively, of Figure 5. The similarity in the active site residues and overall geometry of the active sites of isopropylmalate dehydrogenase and isocitrate dehydrogenase is remarkable, as is the similarity to the active site of malic enzyme. The tyrosine and lysine, as putative catalytic residues, are conserved, as is the arginine that hydrogen bonds the α-carboxylate of the substrate, and three of the ligands to the metal ion, two aspartate carboxylates, and a water molecule. In the (*R*)-hydroxyacid family, one of the aspartates that coordinates the metal ion in malic enzyme is replaced by a second water molecule and the two asparagine residues that form a hydrogen bond to the α-carboxylate of the substrate in malic enzyme are replaced with arginine residues. The active site of homoisocitrate dehydrogenase has identical residues, but the tyrosine is away from the lysine. However, the structure is an open form, and it is known that a conformational change is required to close the site upon substrate binding and that the tyrosine is then in the proximity of homoisocitrate (*35, 40*). As shown in Figures 2 and 3, the overall structure and all of the active site residues are conserved in tartrate dehydrogenase.

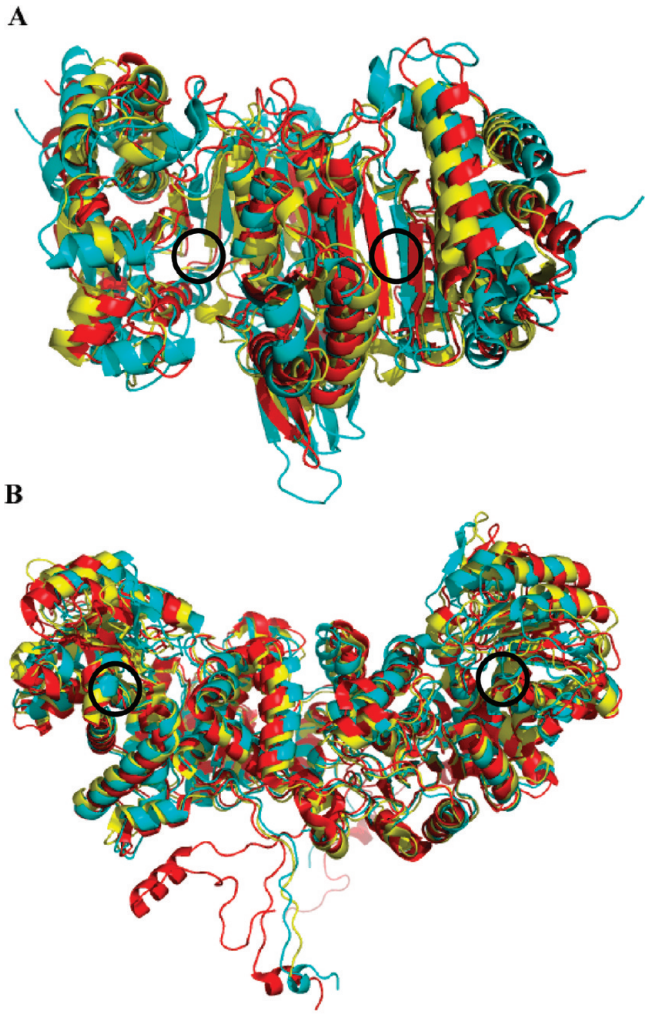


FIGURE 2: Structural overlay. (A) The structures of a dimer of three members of the (*R*)-hydroxyacid family are superimposed. The enzymes are isocitrate dehydrogenase (cyan), isopropylmalate dehydrogenase [red, Protein Data Bank (PDB) entry 1A05], and homoisocitrate dehydrogenase (yellow, PDB entry 1X0L). (B) *Ascaris* malic enzyme (red, PDB entry 1LLQ), pigeon liver malic enzyme (cyan, PDB entry 1GQ2), and human malic enzyme (yellow, PDB entry 1PJ2) are superimposed. The locations of the active sites are shown with a circle. The figures were generated using the PyMOL molecular visualization program (http://pymol.sourceforge.net/).

The three-dimensional arrangement of active site residues is identical in isopropylmalate dehydrogenase and isocitrate dehydrogenase, and in fact, the two can be superposed (Figure 6A). The homoisocitrate dehydrogenase active site will likely also be identical with Mg-homoisocitrate bound. This is not surprising given the similarity of the overall fold and complete conservation of all active site residues. The three-dimensional arrangement of active site residues in the malic enzymes is very similar to that of isocitrate dehydrogenase, but the active sites are mirror images (Figure 6B). This is consistent with the opposite stereochemistry at the Cα alcohol of L-malate and D-isocitrate (and isopropylmalate). One of the water molecules in the metal ion coordination sphere in the (*R*)-hydroxyacid family takes the place of D279 in malic enzyme. The distance between the active site lysine ε-amine and tyrosine phenolic hydroxyl in the binary complex of malic enzyme is 3.3 Å (*41*) but decreases to 2.9 Å in the closed quaternary E−NADH−Mg−oxalate complex form (*37*). In the quaternary E−NADH−Mg−oxalate complex, the distance from the lysine ε-amine and the malate α-hydroxyl is 2.8 Å, and it is thus set to act as a base in the overall reaction. The tyrosine phenolic hydroxyl is also in position to donate a proton to C3 of enolpyruvate. In the isocitrate dehydrogenase and isopropylmalate dehydrogenase ternary E−$M^{2+}$−substrate complexes, the distance between the active site lysine ε-amine and the tyrosine phenolic hydroxyl is ∼3.7 Å, similar to that found in the open form of the malic enzymes, while the distance between the lysine ε-amine and the substrate α-hydroxyl is ∼3.5 Å, which is expected to be within hydrogen bonding distance in the closed form of the enzyme (*27, 34*). In addition to the difference in the active site stereochemistry between the malic enzymes and (*R*)-hydroxyacid family, there are two other differences. First, the malic enzymes have a catalytic aspartate (D278 in the human enzyme; see Acid−Base Chemical Mechanism) that is absent in the (*R*)-hydroxyacid family. Second, two asparagine residues and an arginine are hydrogen-bonded to the substrate α-carboxylate in the malic enzymes, while there are three arginine residues in the case of the (*R*)-hydroxyacid family. These changes almost certainly contribute to the catalytic mechanism in these two subfamilies.

Details of the mechanism are discussed below. We begin with a discussion of the mechanism of the malic enzymes and then discuss similarities and differences between the two families. Although the exact mechanism of the other oxidative decarboxylases (tartrate dehydrogenase and isopropylmalate dehydrogenase) has not yet been determined, the arrangement of their active site residues and their spatial positions in those enzymes are very similar to those that have been well studied. Their chemical mechanisms are thus likely to be very similar to those discussed in detail below.

## ACID−BASE CHEMICAL MECHANISM

*Malic Enzyme.* The malic enzymes are perhaps the best studied of any member of the class of pyridine dinucleotide-linked, metal ion-dependent β-hydroxyacid oxidative decarboxylases. The proposed acid−base mechanism is based on extensive kinetic studies, including pH−rate profiles (*42*−*44*) and isotope effects (*45*−*51*), structural studies (*36, 37, 41, 52*−*54*), and site-directed mutagenesis (*25, 29, 55, 56*). The current general acid−general base chemical mechanism was proposed on the basis of the E−NADH−Mn−malate structure (*37*) and site-directed mutagenesis studies of Karsten et al. (*29*). The mechanism proceeds via the use of a catalytic triad.

In the open form of the enzyme, the active site lysine is within hydrogen bonding distance of an active site aspartate, but not of the active site tyrosine. The structure of the closed form of the human and *Ascaris* NAD-malic enzymes (*37, 52*), with cofactor, metal ion, and substrate (or substrate analogue) bound, shows the active site lysine within hydrogen bonding distance of the substrate hydroxyl, and the active site tyrosine, which is properly positioned to deliver a proton to C3 of the enolpyruvate intermediate that results from oxidative decarboxylation. In addition, an aspartate that does not participate in coordination of the metal ion is within strong hydrogen bonding distance of a glutamate that participates in coordinating the metal ion (Figure 5A). There is a net charge of −2 in the active site of the quaternary E−NAD−$M^{2+}$−malate complex. Four side chain carboxylates and the substrate carboxylates are partially balanced

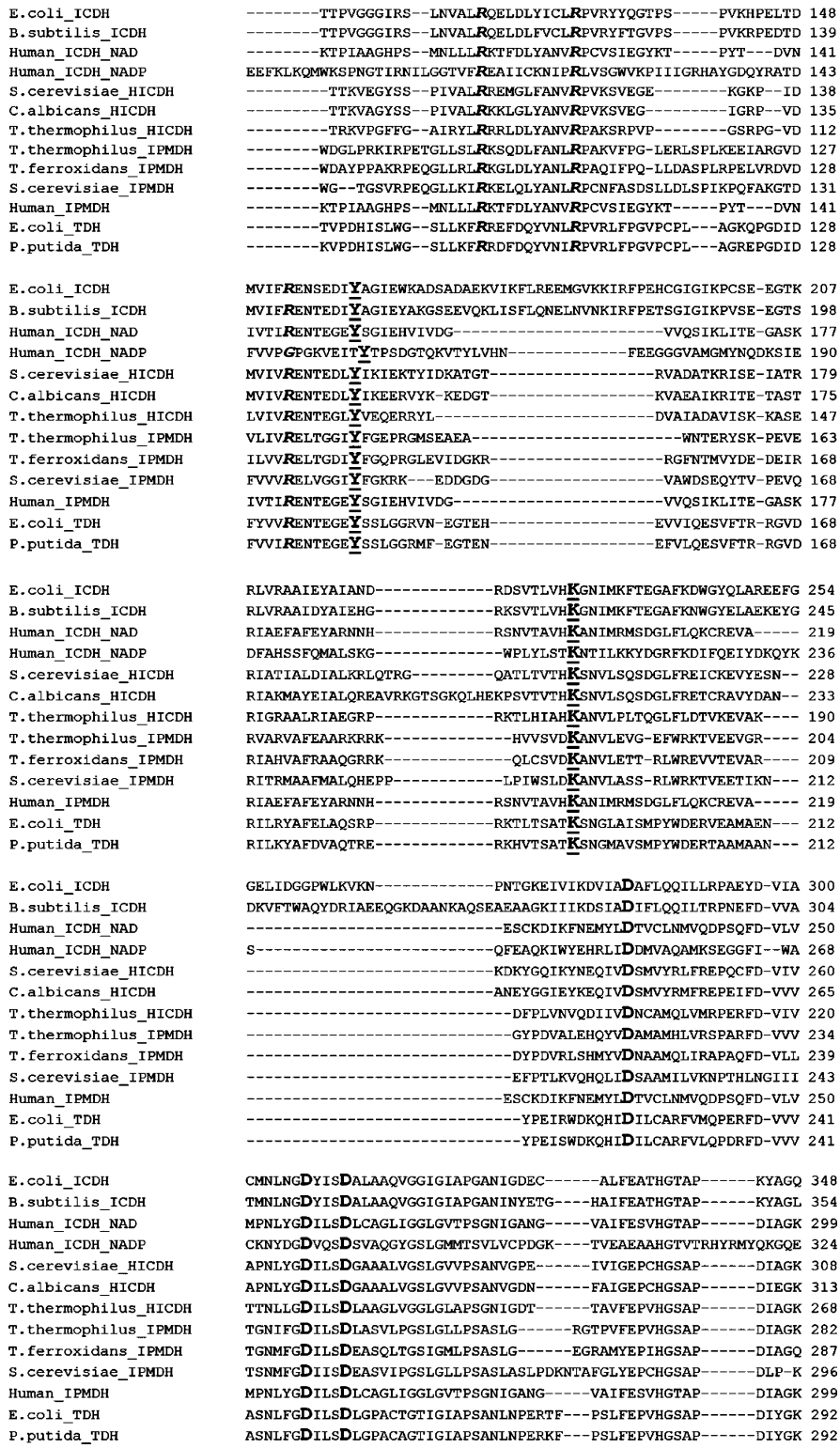


FIGURE 3: Multiple-sequence alignment for isocitrate dehydrogenase, isopropylmalate dehydrogenase, homoisocitrate dehydrogenase, and tartrate dehydrogenase, showing important conserved residues. The residues coordinating the metal ion are in bold, while the residues coordinating the substrate are bold and italicized. The catalytic residues are bold and underlined. The multiple-sequence alignment was created using ClustalW (http://www.ebi.ac.uk/Tools/clustalw/) (*39*).

by the charge on the metal ion, the arginine that ion pairs the substrate α-carboxylate, the charge on the pyridine ring of the cofactor, and the charge of the catalytic lysine, giving a net charge of −2 on the basis of these residues (Table 1). Lysine requires assistance to act as a base, and this is supplied by the aspartate that is in the proximity of the glutamate, which serves as a ligand to the metal ion (Figure 7).

The proposed mechanism of the *Ascaris* NAD-malic enzyme reaction, as an example, is shown in Figure 8 (*29*). A catalytic triad, comprised of K199, Y126, and D294, was proposed to function for the malic enzymes. The pH dependence of $V/K_{malate}$ decreases at low pH, giving a global p$K_a$ of 5.6 reflecting the general base. Given the net negative active site (Table 1), the initial hydrogen bonding of K199

```
Pigeon            LFYKVLTSDIERFXPIVYTPTVGLACQHYGLAFRRPRGLFITIHDR--GHIATXLQSWPE 130
D.melanogaster    LFYNVLSSDIGYMMPLVYTPTVGLACQRYSLIHQNAKGMFISIKDK--GHIYDVLKNWPE 160
Human             LFYRILQDDIESLMPIVYTPTVGLACSQYGHIFRRPKGLFISISDR--GHVRSIVDNWPE 152
A.suum            LFYRVVCDHVKELMPIVYTPTVGLACQNFGYIYRKPKGLYITINDNSVSKIYQILSNWHE 168
C.elegans         LYYRVLCDNVKELMPIVYTPTVGQACQHFGFIYRNPKGLYITINDNSISKIHQILANWPT 180

Pigeon            SVIKAIVVTDGERILGLGDLGCYGXGIPVGKLALYTACGGVKPHQCLPVXLDVGTDNETL 190
D.melanogaster    TDVRAIVVTDGERILGLGDLGANGMGIPVGKLSLYTALAGIKPSQCLPITLDVGTNTESI 220
Human             NHVKAVVVTDGERILGLGDLGVYGMGIPVGKLCLYTACAGIRPDRCLPVCIDVGTDNIAL 212
A.suum            EDVRAIVVTDGERILGLGDLGAYGIGIPVGKLALYVALGGVQPKWCLPVLLDVGTNNMDL 228
C.elegans         ENVRAIVITDGERILGLGDLGTYGIGIPVGKLALYVALAGIRPEWCLPVILDVGTDNSEL 240

Pigeon            LKDPLYIGLRHKRIRGQAYDDLLDEFXEAVTSRYGXNCLIQFEDFANANAFRLLHKYRNK 250
D.melanogaster    LEDPLYIGLRERRATGDLYDEFIDEFMHACVRRFGQNCLIQFEDFANANAFRLLSKYRDS 280
Human             LKDPFYMGLYQKRDRTQQYDDLIDEFMKAITDRYGRNTLIQFEDFGNHNAFRFLRKYREK 272
A.suum            LNDPFYIGLRHKRVRGKDYDTLLDNFMKACTKKYGQKTLIQFEDFANPNAFRLLDKYQDK 288
C.elegans         LNDPFYTGLRRKRVRGPEYDTLVDNFMKAATKRFGRDTLIQFEDFGNQNAYRLLDRYKGE 300

Pigeon            YCTFNDDIQGTASVAVAGLLAALRITKNRLSDHTVLFQGAGEAALGIANLIVXAXQKEGV 310
D.melanogaster    FCTFNDDIQGTASVAVAGLLASLKIKKTQLKDNTLLFLGAGEAALGIANLCLMAMKVEGL 340
Human             YCTFNDDIQGTAAVALAGLLAAQKVISKPISEHKILFLGAGEAALGIANLIVMSMVENGL 332
A.suum            YTMFNDDIQGTASVIVAGLLTCTRVTKKLVSQEKYLFFGAGAASTGIAEMIVHQMQNEGI 348
C.elegans         YCMFNDDIQGTAAVVVAGLLASTRITKKKLSQERIVFLGAGGAATGVAEMCVRQMMDEGL 360

Pigeon            VAAIGGAFTQQILQDXAAFNKRPIIFALSNPTSKAECTAEQLYKYTEGRGIFASGSPFDP 426
D.melanogaster    AAAQGGAFNQEILELMADINETPIIFALSNPTSKAECTAEEAYTYTKGRCIFASGSPFAP 458
Human             VAGAGRLFTPDVIRAMASINERPVIFALSNPTAQAECTAEEAYTLTEGRCLFASGSPFGP 451
A.suum            ASTVRGAFNEEVIRAMAEINERPIIFALSNPTSKAECTAEEAYTFTNGAALYASGSPFPN 464
C.elegans         ASTVAGAFTEDIIKEMARLNPRPIIFALSNPTSKAECTAETAYRCTNGAVLFASGSPFEN 477

Pigeon            VTLPSGQTLYPGQGNNSYVFPGVALGVISCGLKHIGDDVFLTTAEVIAQEVSEENLQEG- 485
D.melanogaster    VTYNN-KKFYPGQGNNSYIFPGVALGVLCAGMLNIPEQVFLVAAERLAELVSKDDLAKG- 516
Human             VKLTDGRVFTPGQGNNVYIFPGVALAVILCNTRHISDSVFLEAAKALTSQLTDEELAQG- 510
A.suum            FELNG-HTYKPGQGNNAYIFPGVALGTILFQIRHVDNDLFLLAAKKVASCVTEDSLKVG- 522
C.elegans         VEMNG-KLYKPGQGNNAYIFPGVALGAVLFRTKNIPDKLFLLAARMVAEAVSEKSLNTYS 536
```

FIGURE 4: Multiple-sequence alignment for NAD-malic enzymes from several different organisms, showing important conserved residues. Residues coordinating the metal ion are bold, while residues coordinating the substrate are bold and italicized. The catalytic residues are bold and underlined. The-multiple sequence alignment was created using ClustalW (*39*).

and D294 in the open form and the close approach of D294 and E271 in the closed form suggest a strong hydrogen bond between D294 and E271, and a neutral K199 that can serve as a base, as suggested in Figure 8 (II). The lysine then serves to accept a proton from the hydroxyl of malate in the oxidation step to generate the oxaloacetate intermediate (III). Prior to oxidation to the ketone, malate is bound with its C4 carboxylate in the C2−C3 plane, and this conformation does not favor decarboxylation. However, after hydride transfer, the C4 carboxylate of malate is perpendicular to the C2−C3 plane, generating more favorable molecular orbital overlap. The $\beta$-ketoacid is then activated for decarboxylation, and the majority of catalysis of this step is provided by the metal ion, acting as a Lewis acid to produce enolpyruvate, with K199 donating a proton to the enol oxygen (IV). (The protonated base, K199, could also stabilize the enolate without a formal proton transfer, but the p$K_a$ of the enolate is higher than that of K199, favoring proton transfer to form the enol.) In agreement, kinetic $^{13}$C isotope effects measured for divalent metal ion-catalyzed decarboxylation of oxaloacetate are very similar to the intrinsic $^{13}$C kinetic isotope effects for decarboxylation of the oxaloacetate intermediate in the malic enzyme reaction, suggesting the enzyme simply provides the site for binding metal ion and reactant and plays only a small catalytic role in this step of the reaction (*57*). Finally, tautomerization of enolpyruvate to pyruvate proceeds via general base−general acid catalysis, with K199 accepting a proton from the enol and Y126 donating a proton to C3 to give pyruvate (V). Release of products and proton rearrangement give the catalytic triad in the same protonation state as at the beginning of the reaction (VI).

The deuterium isotope effect, measured with L-malate-2-D, on $V$ is 2.0, slightly greater than the effect of 1.6 on $V/K_{malate}$, suggesting that oxidative decarboxylation contributes significantly to rate limitation at saturating reactant concentrations (*47*). Pre-steady-state kinetic studies further exhibit a lag in the time course for the appearance of NADH, attributed to isomerization of the E−NAD binary complex prior to binding malate (*58*). Taken together, data indicate chemistry and the E−NAD isomerization contribute equally to rate limitation of the overall reaction.

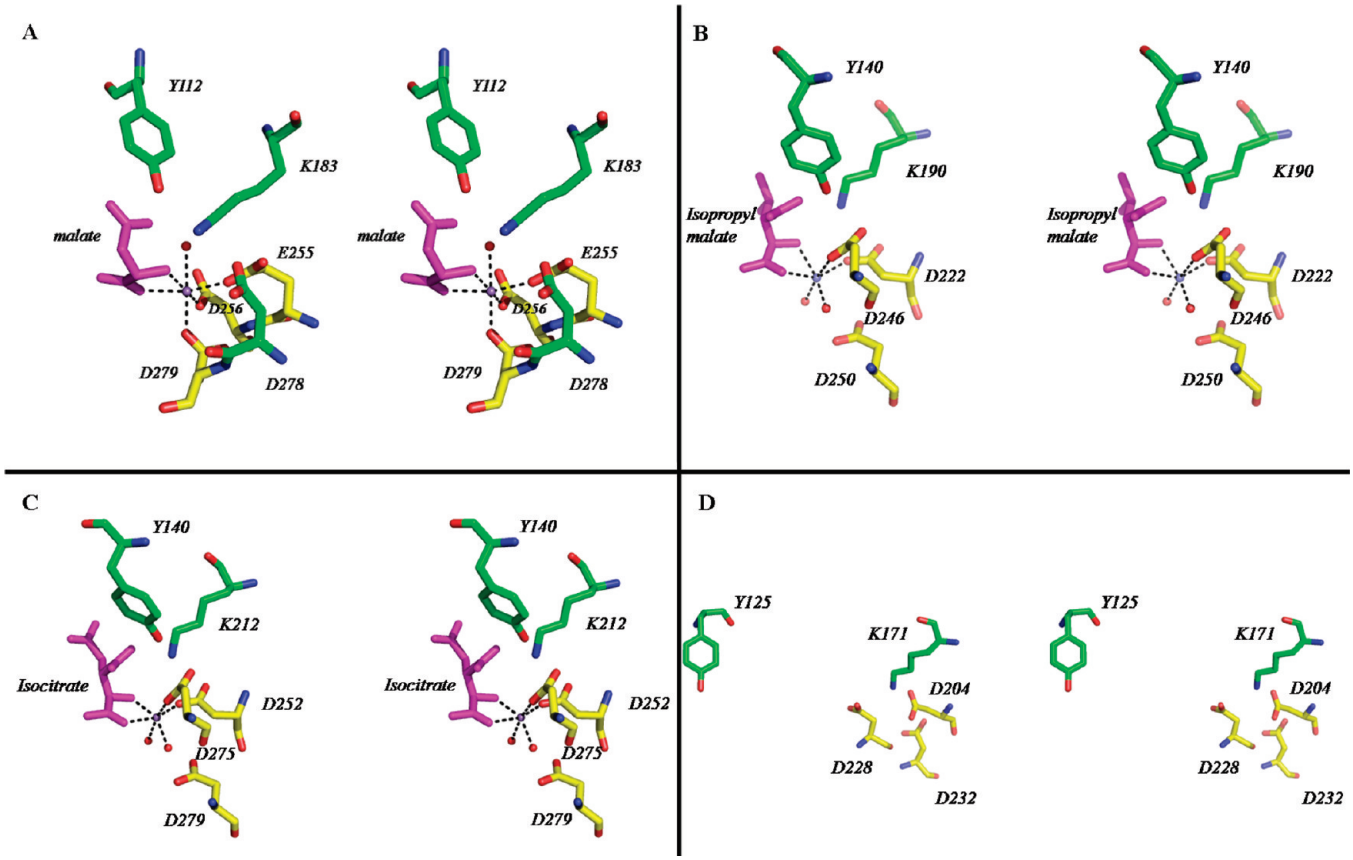


FIGURE 5: Close-up view of active sites in stereo mode. Enzymes with active sites pictured are (A) malic enzyme, (B) isopropylmalate dehydrogenase, (C) isocitrate dehydrogenase, and (D) homoisocitrate dehydrogenase. Residues that coordinate the metal ion are shown; the metal ion is colored purple, and coordinating residues are colored yellow. Substrates are colored magenta. The structures for malic enzyme and homoisocitrate dehydrogenase are the open conformations. Panels A−D are PDB entries 1PJ2, 1A05, 1LWD, and 1X0L, respectively. This figure was generated using the PyMOL molecular visualization program.

In support of the proposed mechanism are the structural studies cited above and studies of site-directed mutations of the three participants in the catalytic triad (*29*). Mutation of K199 to A gave a $10^5$-fold decrease in $k_{cat}$ (*56*), while mutation to R gave a 10-fold decrease in $k_{cat}$, but no change in the p$K_a$ of the putative general base. However, mutation of D294, which is very close to E271, to A gave a 13000-fold decrease in the rate, and a shift in the p$K_a$ on the acid side to ~9.7 from 5.6. Correcting for the contribution of the E−NAD isomerization (see above), we find the decrease in the rate of the chemical steps is >25000-fold. Thus, removal of the auxiliary catalyst that is required to deprotonate K199 so that it can serve as a base results in a pH dependence that is expected if K199 were acting alone.

Tautomerization is generally very fast compared to other steps along the malic enzyme reaction pathway, and as a result, the p$K_a$ for Y126 is not observed in the pH−rate profiles. Mutation of Y126 to F gives a 60000-fold reduction in the rate, consistent with its important role in catalysis. Correcting for the contribution of the E−NAD isomerization (see above), we find the decrease in the rate of the chemical steps is >120000-fold. However, the p$K_a$ of the general base, D294, in the Y126F mutant enzyme is still 5.6, identical to that of the wild-type enzyme.

For the sake of comparison, the mechanism of the metal ion-independent 6-phosphogluconate dehydrogenase (6PGDH) is shown in Figure 9. The acid base catalytic groups, K183 and E190, are shown with K183 within hydrogen bonding distance of the 3-hydroxyl group of 6PG, and E190 in the vicinity of the 1-carboxylate of the substrate. The substrate binds to the enzyme form with K183 neutral and E190 protonated; i.e., the two groups are in reverse protonation states (I). The p$K_a$ values observed in the pH−rate profiles of the wild-type enzyme are ~7 and ~8 for groups that must be unprotonated and protonated, respectively (*59, 60*). The fraction of active enzyme in the pH-independent region is equal to antilog(p$K_1$ − p$K_2$) = 0.1, given the reverse protonation state between the two groups. However, it is important in the overall reaction to utilize K183 and not E190 as the base in the reaction. Oxidation of the substrate to 3-keto-6PG occurs via hydride transfer to NADP, and proton transfer to K183. Reduction of the nicotinamide ring results in its rotation by 90°, causing the 1-carboxylate to move away from E190 (*61*). Protonated K183 now acts to polarize the carbonyl of the ketone, facilitating decarboxylation to give the 1,2-enol of ribulose 5-phosphate. Tautomerization of the enol to the ketone is catalyzed by K183 accepting a proton from the enol and E190 donating a proton to C1 to give ribulose 5-phosphate. Thus, although the overall reaction is the same, the catalytic mechanism differs significantly from that of the (*R*)-hydroxyacid and (*S*)-hydroxyacid families.

Given the similarity in the active sites of the (*R*)-hydroxyacid family to that of the (*S*)-hydroxyacid family (malic enzyme), it is highly likely the same general mechanism applies in all cases. Of the enzymes in the (*R*)-hydroxyacid family, isocitrate dehydrogenase has been well studied; data for homoisocitrate dehydrogenase and tartrate dehydrogenase are not as extensive, and only structural data

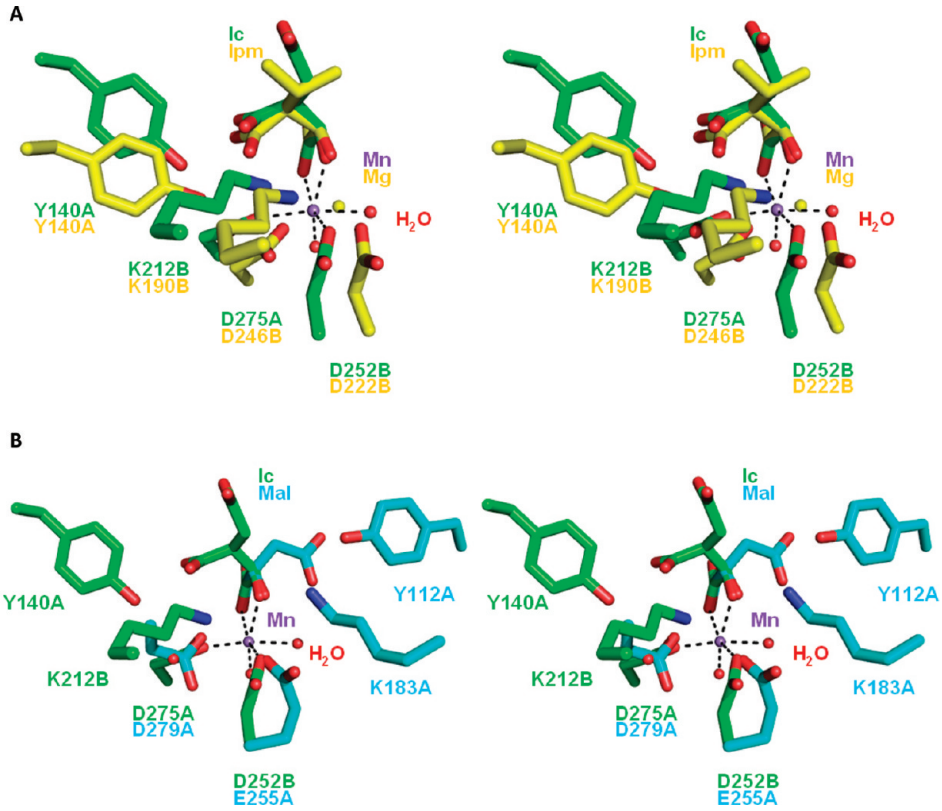


FIGURE 6: Stereoview of active site superpositions. (A) The active sites of isocitrate dehydrogenase (PDB entry 1LWD) and isopropylmalate dehydrogenase (PDB entry 1A05) are colored green and yellow, respectively. The metal ion is shown as a purple sphere (yellow for Mg), and water molecules are shown as red spheres. (B) The active sites of isocitrate dehydrogenase and malic enzyme (PDB entry 1PJ2) are colored green and cyan, respectively. Coordination bonds to the metal ion are shown for one of the enzymes in both panels A and B.

Table 1: Net Charges of the Active Sites of Metal Ion-Dependent Oxidative Decarboxylases

| | malic enzyme | isopropylmalate dehydrogenase | isocitrate dehydrogenase | homoisocitrate dehydrogenase | tartrate dehydrogenase |
|---|---|---|---|---|---|
| substrate | −2 | −2 | −3 | −3 | −2 |
| Asp | 3 × −1 = −3 | 3 × −1 = −3 | 3 × −1 = −3 | 3 × −1 = −3 | 3 × −1 = −3 |
| Glu | −1 | none | none | none | none |
| $K^+$ | none | none | none | +1 | +1 |
| $NAD^+$ | +1 | +1 | +1 | +1 | +1 |
| Arg | +1 | 3 × +1 = +3 | 3 × +1 = +3 | 3 × +1 = +3 | 3 × +1 = +3 |
| $Mg^{2+}$ | +2 | +2 | +2 | +2 | +2 |
| net charge | −2 | +1 | 0 | +1 | +2 |

are available for isopropylmalate dehydrogenase. Each of these enzymes will be discussed below in terms of the mechanism proposed for the malic enzymes.

*Isocitrate Deydrogenase.* The porcine isocitrate dehydrogenase has been extensively studied. The overall mechanism of the enzyme follows that shown in Scheme 1. We propose that, as is true for the malic enzymes, the acid−base chemistry of the isocitrate dehydrogenase overall reaction is catalyzed by an active site lysine-tyrosine pair. On the basis of available structures (*24, 27, 62, 63*), kinetic studies, and site-directed mutagenesis (*24, 26*−*28, 58, 64*−*66*), a mechanism has been proposed for isocitrate dehydrogenase. The wild-type enzyme exhibits a p$K_a$ of ∼5.2 for a group that must be unprotonated for optimal activity (*28*). The p$K_a$ was assigned to the ionization of the metal-bound hydroxyl of isocitrate. Tyrosine 140, which corresponds to Y126 in the *Ascaris* malic enzyme, was proposed to be the general acid that protonates the enol to give α-ketoglutarate (*64*). Below, the proposed mechanism will first be considered, and then data obtained for isocitrate dehydrogenase will be considered in terms of a catalytically active Lys-Tyr pair.

Data support the proposed role of Y140 as the general acid that must protonate the enol of α-ketoglutarate to generate the ketone product (*64*). Changing the tyrosine to a side chain that cannot function over the pH range of 5−9, i.e., phenylalanine which is missing the phenolic hydroxyl and threonine which has a p$K_a$ of >14, results in a very low pH-independent basal activity that is 400-fold lower than that of the wild type. A change to glutamate and lysine gives enzymes that exhibit pH dependence with observed p$K_a$ values of 6.4 and 6.75, respectively, for a group that must be protonated for optimal activity. Finally, the detritiation of α-ketoglutarate requires the presence of Y140.

Data are not as clear in the assignment of the group with a p$K_a$ of 5.2 observed in the $k_{cat}$ profile of the wild-type enzyme. Changing K212 to Q, which does not allow it to function as a base, does not eliminate the pH dependence of $k_{cat}$ but does give a 540-fold decrease in the rate and a shift in the p$K_a$ to 7.5; a pH-independent basal level of activity ∼1000-fold lower than that of the wild type is observed at pH <6.5. On the other hand, a change to *R* gives an only 10-fold change, and no change in the observed p$K_a$, similar

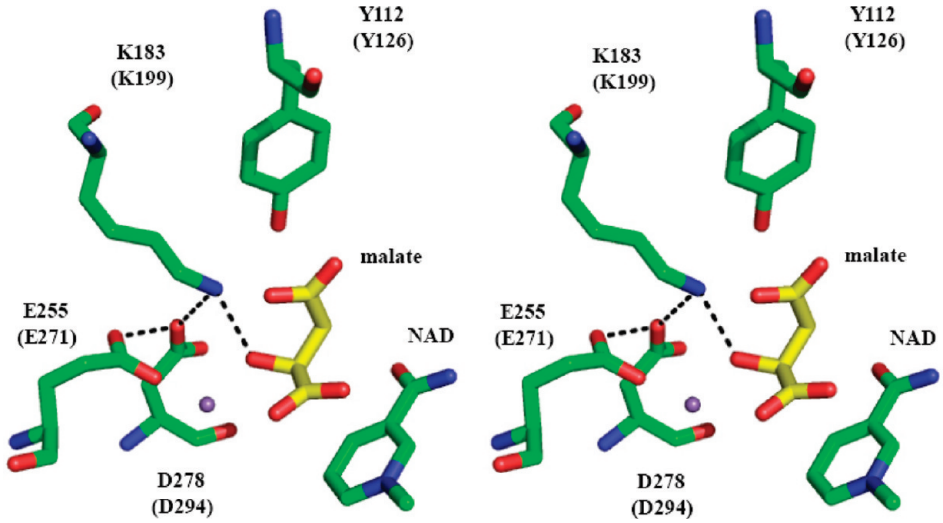


FIGURE 7: Stereoview of active site structure and catalytic triad in the human malic enzyme (PDB entry 1PJ2). The corresponding residues for the *Ascaris* malic enzyme are shown in parentheses. Distances between K183 and D278 (2.8 Å), the malate 2′-OH group and K183 (2.78 Å), and E255 and D278 (2.6 Å) in the closed structure are shown. $Mn^{2+}$ is shown as a purple sphere. The figures are generated using the PyMOL molecular visualization program.

to the behavior of malic enzyme (*29*). Clearly, the observed p$K_a$ does not reflect K212, but its value is influenced by the positively charged side chain in agreement with the authors' suggestion (*64*). The lysine side chain must have a function in the reaction in addition to an electrostatic effect on the p$K_a$ of another group, however, since the activity is decreased >500-fold. Two other lines of evidence are used to assign the p$K_a$ of 5.2 to the hydroxyl of isocitrate, viz., site-directed mutagenesis to change conserved active site aspartate side chains and replacement of the metal ion that chelates isocitrate (*28*). On the basis of structural data, two of the aspartate residues serve as ligands to the metal ion in the active site, D252 and D275, while the third, D279, is in the vicinity of the metal−isocitrate complex and hydrogen-bonded to two water molecules (*52*). Replacement of D252 or D275 with cysteine gives similar p$K_a$ values for $k_{cat}$ but a decrease in rate of 3.6- or 2.7-fold, respectively, consistent with a change in the electronic properties of the metal ion, which must serve as a Lewis acid in the decarboxylation reaction. Of interest, the observed p$K_a$ is unchanged, which is not consistent with the ionization of the metal-bound hydroxyl of isocitrate. Replacement of D279 with C, however, gives a lower p$K_a$ of 4.7, and a 240-fold lower rate, consistent with the weaker hydrogen bonding ability of the cysteine thiol(ate). Metal ion replacement, e.g., $Mn^{2+}$ to $Co^{2+}$, gave observed p$K_a$ values in $k_{cat}$ of 5.24 and 5.07, which the authors suggest are significantly different in support of ionization of the metal-coordinated isocitrate hydroxyl (*28*). The p$K_a$ values 5.24 and 5.07 are likely actually within error equal.[1] In agreement, a similar metal replacement study by Auld and Valee (*67*) gave a shift in the p$K_a$ of carboxypeptidase from 6.36 to 5.33 as expected given the p$K_a$ values of 10.6 and 9.7 for hydrolysis of $(Mn\text{-}OH_2)^{2+}$ and $(Co\text{-}OH_2)^{2+}$, respectively (*68*). Also interestingly, changing R110 and R133 (within hydrogen bonding distance of the substrate α-carboxylate of isocitrate) to Q results in increasing the p$K_a$ in the $k_{cat}$ pH−rate profile to 6.4 and 7.4, respectively (*52*). Thus, positive charge in the active site is clearly important.

If the p$K_a$ observed in the $k_{cat}$ pH−rate profile is not that of the metal-isocitrate hydroxyl, how can the data be reconciled? It is likely given the close similarity in the active sites of the MEs and the (*R*)-hydroxyacid family that the lysine-tyrosine pair functions in an acid−base role in isocitrate dehydrogenase as in the case of malic enzyme. However, it is clear that the residue responsible for the p$K_a$ in the $k_{cat}$ pH−rate profile is not lysine but is influenced greatly by its environment. Specifically, a decrease in positive charge results in an increase in the p$K_a$, suggesting either a positively charged group in the vicinity of K212, which would have a lower p$K_a$ as a result of electrostatic repulsion of the two groups when protonated, or a neutral acid, which would be preferentially ionized in a positive site. The only positively charged groups in the active site, besides K212 and the metal ion, are the three arginine residues in the vicinity of the substrate α-carboxylate and the nicotinamide of $NAD^+$. However, D279 or one of the other aspartate side chains, either directly or via hydrogen-bonded water, could certainly function to deprontonate K212 in a manner similar to that proposed for malic enzyme. In this regard, one must remember that the structure available is that of the E−Mn−isocitrate complex. It is possible, for example, that one of the two aspartates that serve as metal ion ligands serves as a catalyst to deprotonate K212 and that D279 acts as a ligand to the metal ion in the quaternary E−NADP−Mn−isocitrate complex. We suggest a triad, similar to that observed for malic enzyme, functions to catalyze the isocitrate oxidative decarboxylation with another active site group, e.g., an aspartate, required to deprotonate K212, which functions as the general base to deprotonate the isocitrate hydroxyl, while Y140 functions as the general acid to protonate the enol. Elimination of positive charge in the site will cause an increase in the p$K_a$ of the aspartate, while elimination of the aspartate will give the p$K_a$ of the lysine unless the new side chain can function as a base, as in H or

[1] Standard errors obtained are too low given the data reported by the authors. On the basis of hundreds of pH−rate profiles obtained by PFC, the standard errors on the p$K_a$ values are likely ~0.2. It is likely that at least a portion of the difference results from log to ln conversions, in the error analysis.

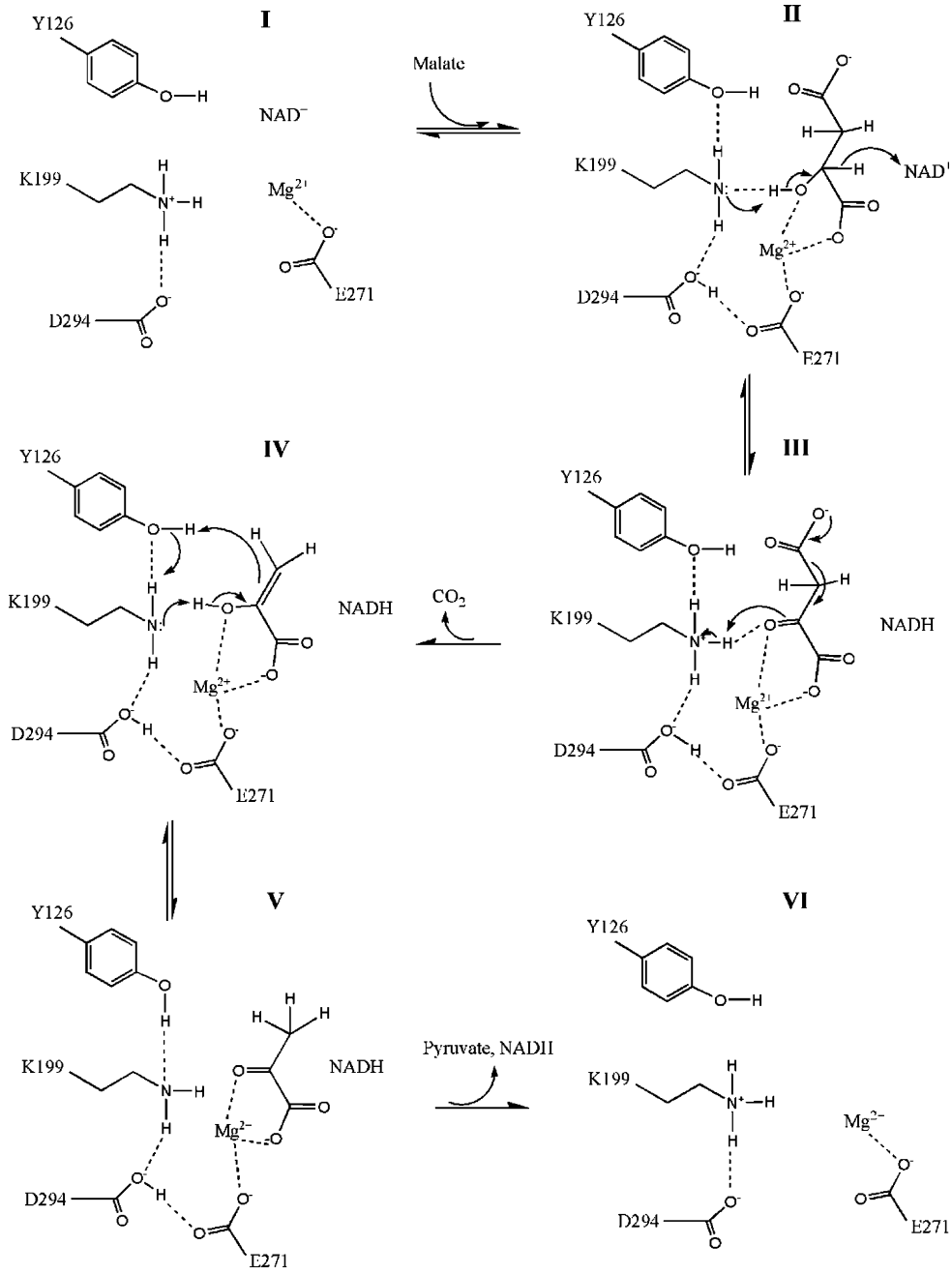


FIGURE 8: Proposed general acid−general base mechanism for *A. suum* malic enzyme (*29*).

C. The proposed mechanism also explains the relatively high activity observed for the K212R mutant enzyme. The p$K_a$ of the $\delta$-guanidinium of arginine is 2 pH units higher than that of the $\varepsilon$-amine of lysine, and thus, one might expect a 100-fold decrease in the rate with R212 as the base catalyst in place of K212, and not the 10-fold change observed. However, the chemical steps do not contribute to rate limitation in the case of the wild-type enzyme and must be at least 10 times faster than structural changes required to set up the site for catalysis. In agreement, on the basis of the pH dependence of isotope effects, Grissom and Cleland estimate that catalysis is 16 times faster than substrate dissociation (*57*).

The lack of a deuterium isotope effect on *V* indicates the chemical steps contribute even less than they do at limiting reactant concentrations (*V*/*K*). Data indicate the rate of the chemical steps under *V*/*K* conditions must be decreased by >8500-fold (16 × 540-fold; $K_m$ values do not change for K212Q compared to the wild type). However, on the basis of initial rate and isotope exchange at equilibrium, the rate of release of NADPH is much slower than the rate of release of isocitrate, and thus, the rate of the chemical steps must be decreased by >$10^4$-fold (*19, 20*).

A pH-independent basal level of activity was observed for several mutant enzymes. The K212Q mutant enzyme exhibits a 1000-fold lower rate than the $k_{cat}$ of the wild-type enzyme at pH <6.5. The Y140F and Y140T mutant enzymes exhibit a 400-fold lower rate than the wild-type enzyme over the pH range of 5−9. The basal activity is still much greater than that of the uncatalyzed reaction and must be due to a combination of catalysis by the remaining catalytic group, water, and the metal ion. A series of double mutations could be used to sort this out using a mutant cycle analysis.

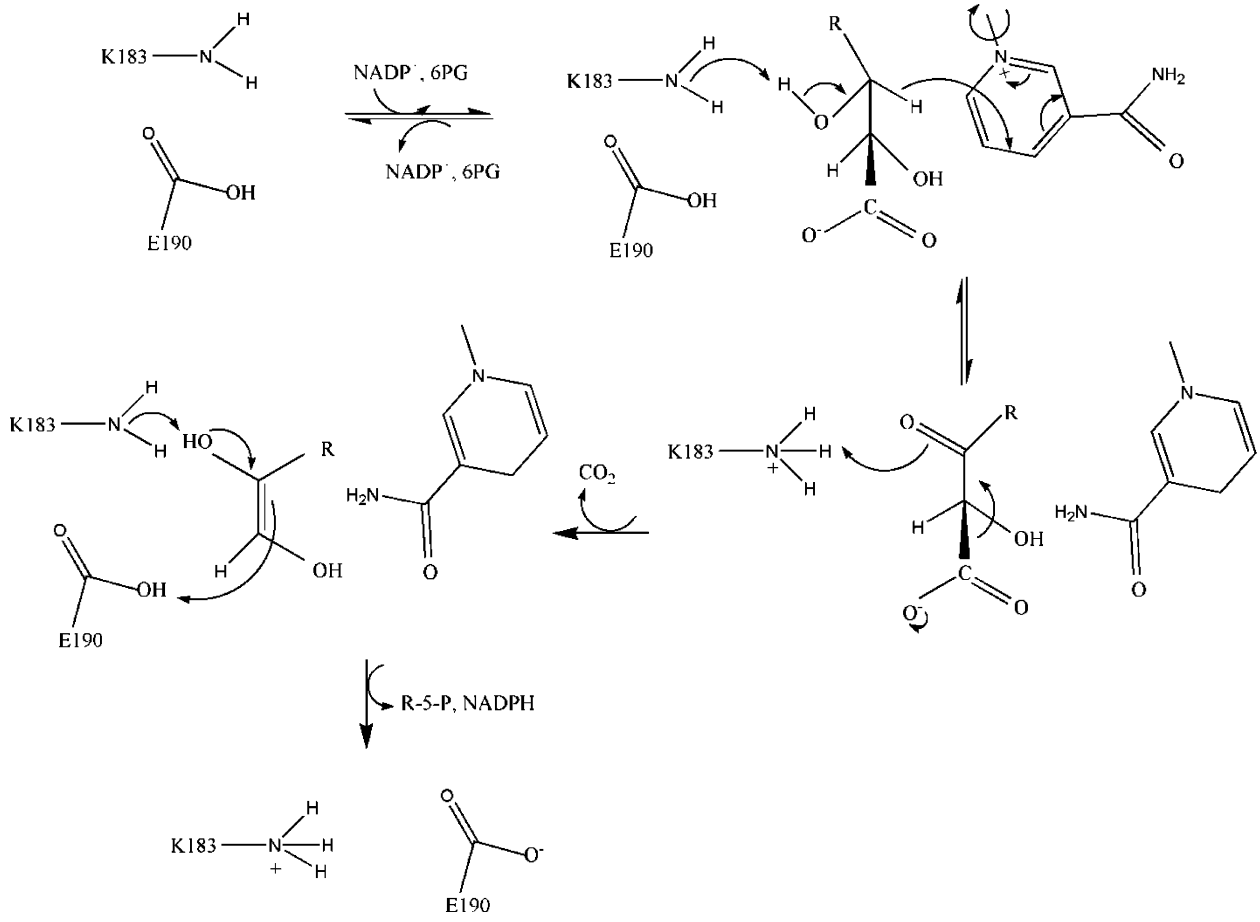


FIGURE 9: Proposed general acid−general base mechanism for sheep liver 6-phosphogluconate dehydrogenase (*59, 60*).

*Homoisocitrate Dehydrogenase.* Data obtained for the homoisocitrate dehydrogenase reaction are also consistent with the action of a lysine-tyrosine pair, as suggested by the active site structure of the enzyme. $k_{cat}$ decreases at low pH, giving a p$K_a$ of ~6.5, and decreases at high pH above a p$K_a$ of ~9.5 (*40*). Isocitrate is a slow substrate for homoisocitrate dehydrogenase and was very useful in interpreting the pH−rate profiles in general. A single base was observed in the $k_{cat}$ and $k_{cat}/K_{Ic}$ profiles with a p$K_a$ of ~7. Data were interpreted in terms of a group with a p$K_a$ of 6.5 that acts as a general base in the hydride transfer step and a group with a p$K_a$ of 9.5 that acts as a general acid to protonate C3 in the tautomerization reaction.

Deuterium isotope effects of unity on $V$ and $V/K_{HIc}$, obtained with homocitrate-2-D, indicate hydride transfer does not contribute to rate limitation (*40*); a small $^{13}(V/K_{HIc})$ of 1.0057 was measured in the same study. Given the value of ~1.05 estimated for the intrinsic $^{13}C$ isotope effect in the malic enzyme reaction, and assuming a similar value in the homoisocitrate dehydrogenase reaction, the chemical step must be at least 10-fold faster than a physical step along the reaction pathway. Solvent deuterium isotope effects suggest this step is a conformational change of the E−NAD−MgHIc complex.

Site-directed mutagenesis of K206 and Y150 resulted in dramatic decreases in rates and in changes in the pH−rate profiles. The $k_{cat}$ values of the K206M and Y150F mutant enzymes at pH 7.5 are decreased by ~2400- and ~680-fold, respectively, compared to that of wild-type HIcDH; the $K_m$ for HIc does not change significantly. The $k_{cat}$ for the K206M mutant enzyme is pH-independent at pH <6 and decrease to a constant value at pH >7. In the case of the Y150F mutant enzyme, $k_{cat}$ is pH-independent at pH >9.5 and decreases to a constant value at pH <8. This behavior can be compared to that of the wild-type enzyme, where $k_{cat}$ decreases at high and low pH, giving p$K_a$ values of ~6.5 and ~9.5. Data are consistent with Y150 acting as a base in the reaction catalyzed by the K206M mutant enzyme and K206 acting as an acid in the Y150F mutant enzyme. The p$K_a$ of Y150 in the absence of K206 is 9.3, while that of K206 in the absence of Y150 is ~6. The most reasonable explanation is the presence of a Lys-Tyr ion pair in the wild-type enzyme with a p$K_a$ of ~7. The low p$K_a$ for K206 in the mutant enzyme likely results from the highly positive nature of the active site, with three arginine residues, the positive charge on NAD, and the metal ion. The pH-independent basal activity exhibited by K206M below pH 8 and Y150F above pH 7 is likely explained as it is for the isocitrate dehydrogenase mutant enzymes (see above).

*Isopropylmalate and Tartrate Dehydrogenases.* There are only limited data available for possible catalytic residues of isopropylmalate dehydrogenase and tartrate dehydrogenase. Miyazaki et al. (*69*) mutated Y139, which corresponds to the general acid in other enzymes, to F in *Thermus thermophilus* isopropylmalate dehydrogenase and observed the $k_{cat}$ was reduced to 7% of that of the wild type, consistent with the importance of the hydroxyl group of the tyrosine in catalysis.

For tartrate dehydrogenase, there is no study that points out the importance of any of the conserved residues; however, as

Table 2: Estimated Decrease in $k_{cat}$ upon Mutation of Catalytic Residues

| mutation | malic enzyme | mutation | isocitrate dehydrogenase | mutation | homoisocitrate dehydrogenase |
|---|---|---|---|---|---|
| K199A | $10^5$ | K212Q | $>10^4$ | K206M | $2.4 \times 10^4$ |
| K199R | 100 | K212R | >100 | | |
| D294A | $1.3 \times 10^4$ | D279C | $>10^4$ | | |
| Y126F | $6 \times 10^4$ | Y140F | $>10^4$ | Y150F | $7 \times 10^3$ |

for isopropylmalate dehydrogenase, the similarity of the arrangement of the lysine-tyrosine pair to the one in the malic enzymes, isocitrate dehydrogenase, homoisocitrate dehydrogenase, and isopropylmalate dehydrogenase, suggests a chemical mechanism very similar to that of the other enzymes.

## OVERALL

All of the metal ion-dependent, pyridine nucleotide-dependent $\beta$-hydroxyacid oxidative decarboxylases utilize a lysine-tyrosine pair to carry out the acid−base catalysis in the oxidation, decarboxylation, and tautomerization steps of the overall reaction. The lysine $\varepsilon$-amine functions as the base in the reaction, and the phenolic hydroxyl of tyrosine functions as the proton donor in the tautomerization reaction; this could occur via the intermediacy of a water molecule for some of the enzymes. However, the way the enzymes utilize the catalytic pair differs. In the case of the malic enzymes and isocitrate dehydrogenase, there is apparently a group, an aspartate carboxylate in the case of malic enzyme, that assists in generating the neutral amine, while for homoisocitrate dehydrogenase, this auxiliary catalyst is not utilized and the lysine-tyrosine pair functions directly. Some of the differences are almost certainly due to the amount of positive charge in the active sites of the respective enzymes. The malic enzymes have less positive charge because two of the three arginines that interact with the substrate α-carboxylate in the (*R*)-hydroxyacid family are asparagines in the malic enzymes.

Table 2 summarizes the decreases in $k_{cat}$ upon mutation of the lysine and tyrosine thought to participate in the catalytic reaction of the oxidative decarboxylases. In all cases, the decrease is on the order of $10^4-10^5$ fold. The values are remarkably similar and suggest this is the catalytic advantage generated for an acid or base catalyst in these reactions.

A number of enzymes have a lysine and tyrosine in their active sites. This pair of residues provides advantages for enzymes that catalyze acid−base chemistry. Given their equal solution p$K_a$ values of 10.5, the two residues, if in the proximity of each other, can ion pair as $NH_3^+-O^-$ or hydrogen bond as $NH_2\cdots HO$, such that reactant binding can select one form or the other. In addition, since one is a neutral acid and the other a cationic acid, the environment of the active site, once it closes in preparation for catalysis, can generate differences in the p$K_a$ values of the two residues, resulting in a broader pH-independent reaction range.

## ACKNOWLEDGMENT

We thank Dr. Babak Andi for help with Figure 6.

## REFERENCES

1. Ochoa, S., Mehler, A. H., and Kornberg, A. (1947) Reversible oxidative decarboxylation of malic acid. *Fed. Proc. 6*, 282.
2. Ochoa, S., Mehler, A. H., and Kornberg, A. (1948) Biosynthesis of dicarboxylic acids by carbon dioxide fixation. 1. Isolation and properties of an enzyme from pigeon liver catalyzing the reversible oxidative decarboxylation of L-malic acid. *J. Biol. Chem. 174*, 979–1000.
3. Kaufman, S., Korkes, S., and Delcampillo, A. (1951) Biosynthesis of dicarboxylic acids by carbon dioxide fixation. 5. Further study of the malic enzyme of *Lactobacillus arabinosus*. *J. Biol. Chem. 192*, 301–312.
4. Saz, H. J., and Hubbard, J. A. (1957) The oxidative decarboxylation of malate by *Ascaris lumbricoides*. *J. Biol. Chem. 225*, 921–933.
5. Kornberg, A., and Pricer, W. E. (1951) Diphosphopyridine and triphosphopyridine nucleotide isocitric dehydrogenases in yeast. *J. Biol. Chem. 189*, 123–136.
6. Agosin, M., and Weinbach, E. C. (1956) Partial purification and characterization of the isocitric dehydrogenase from *Trypanosoma cruzi*. *Biochim. Biophys. Acta 21*, 117–126.
7. Moyle, J. (1956) Some properties of purified isocitric enzyme. *Biochem. J. 63*, 552–558.
8. Burns, R. O., Umbarger, H. E., and Gross, S. R. (1963) Biosynthesis of leucine. 3. Conversion of α-hydroxy-$\beta$-carboxyisocaproate to α-ketoisocaproate. *Biochemistry 2*, 1053–1058.
9. Hsu, Y. P., and Kohlhaw, G. B. (1980) Leucine biosynthesis in *Saccharomyces cerevisiae*: Purification and characterization of $\beta$-isopropylmalate dehydrogenase. *J. Biol. Chem. 255*, 7255–7260.
10. Strassman, M., and Ceci, L. N. (1965) Enzymatic formation of α-ketoadipic acid from homoisocitric acid. *J. Biol. Chem. 240*, 4357–4361.
11. Rowley, B., and Tucci, A. F. (1970) Homoisocitric dehydrogenase from yeast. *Fed. Proc. 29*, A922–A933.
12. Kohn, L. D., Packman, P. M., Allen, R. H., and Jakoby, W. B. (1968) Tartaric acid metabolism. V. Crystalline tartrate dehydrogenase. *J. Biol. Chem. 243*, 2479–2485.
13. Giffhorn, F., and Kuhn, A. (1983) Purification and characterization of a bifunctional L-(+)-tartrate dehydrogenase-D-(+)-malate dehydrogenase (decarboxylating) from *Rhodopseudomonas sphaeroides*. *J. Bacteriol. 155*, 281–290.
14. Dickens, F., and Glock, G. E. (1951) Direct oxidation of glucose-6-phosphate, 6-phosphogluconate and pentose-5-phosphates by enzymes of animal origin. *Biochem. J. 50*, 81–95.
15. Dyson, J. E. D., Dorazio, R. E., and Hanson, W. H. (1973) Sheep liver 6-phosphogluconate dehydrogenase: Isolation procedure and effect of pH, ionic-strength, and metal-ions on kinetic parameters. *Arch. Biochem. Biophys. 154*, 623–635.
16. Tipton, P. A. (1993) Intermediate partitioning in the tartrate dehydrogenase catalyzed oxidative decarboxylation of D-malate. *Biochemistry 32*, 2822–2827.
17. Park, S. H., Kiick, D. M., Harris, B. G., and Cook, P. F. (1984) Kinetic mechanism in the direction of oxidative decarboxylation for NAD-malic enzyme from *Ascaris suum*. *Biochemistry 23*, 5446–5453.
18. Mallick, S., Harris, B. G., and Cook, P. F. (1991) Kinetic mechanism of NAD-malic enzyme from *Ascaris suum* in the direction of reductive carboxylation. *J. Biol. Chem. 266*, 2732–2738.
19. Uhr, M. L., Thompson, V. W., and Cleland, W. W. (1974) Kinetics of pig heart triphosphopyridine nucleotide isocitrate dehydrogenase. 1. Initial velocity, substrate and product inhibition, and isotope-exchange studies. *J. Biol. Chem. 249*, 2920–2927.
20. Northrop, D. B., and Cleland, W. W. (1974) Kinetics of pig heart triphosphopyridine nucleotide isocitrate dehydrogenase. 2. Dead-end and multiple inhibition studies. *J. Biol. Chem. 249*, 2928–2931.
21. Dean, A. M., and Dvorak, L. (1995) The role of glutamate-87 in the kinetic mechanism of *Thermus thermophilus* isopropylmalate dehydrogenase. *Protein Sci. 4*, 2156–2167.
22. Lin, Y., Alguindigue, S. S., Volkman, J., Nicholas, K. M., West, A. H., and Cook, P. F. (2007) Complete kinetic mechanism of homoisocitrate dehydrogenase from *Saccharomyces cerevisiae*. *Biochemistry 46*, 890–898.
23. Hurley, J. H., Dean, A. M., Koshland, D. E., and Stroud, R. M. (1991) Catalytic mechanism of $NADP^+$-dependent isocitrate dehydrogenase: Implications from the structures of magnesium isocitrate and $NADP^+$ complexes. *Biochemistry 30*, 8671–8678.
24. Bolduc, J. M. (1995) Mutagenesis and laue structures of enzyme intermediates: Isocitrate dehydrogenase. *Science 268*, 1312–1318.
25. Liu, D., Karsten, W. E., and Cook, P. F. (2000) Lysine 199 is the general acid in the NAD-malic enzyme reaction. *Biochemistry 39*, 11955–11960.
26. Grodsky, N. B., Soundar, S., and Colman, R. F. (2000) Evaluation by site-directed mutagenesis of aspartic acid residues in the metal

site of pig heart NADP-dependent isocitrate dehydrogenase. *Biochemistry 39*, 2193–2200.
27. Ceccarelli, C., Grodsky, N. B., Ariyaratne, N., Colman, R. F., and Bahnson, B. J. (2002) Crystal structure of porcine mitochondrial $NADP^+$-dependent isocitrate dehydrogenase complexed with $Mn^{2+}$ and isocitrate: Insights into the enzyme mechanism. *J. Biol. Chem. 277*, 43454–43462.
28. Huang, Y. C., Grodsky, N. B., Kim, T. K., and Colman, R. F. (2004) Ligands of the $Mn^{2+}$ bound to porcine mitochondrial NADP-dependent isocitrate dehydrogenase, as assessed by mutagenesis. *Biochemistry 43*, 2821–2828.
29. Karsten, W. E., Liu, D. L., Rao, G. S. J., Harris, B. G., and Cook, P. F. (2005) A catalytic triad is responsible for acid-base chemistry in the *Ascaris suum* NAD-malic enzyme. *Biochemistry 44*, 3626–3635.
30. Dalziel, K. (1980) Isocitrate dehydrogenase and related oxidative decarboxylases. *FEBS Lett. 117*, K45–K55.
31. Dalziel, K. (1984) Kinetics of oxidative decarboxylases. *NATO ASI Ser., Ser. A 81*, 65–81.
32. Cleland, W. W. (1999) Mechanisms of enzymatic oxidative decarboxylation. *Acc. Chem. Res. 32*, 862–868.
33. Karsten, W. E., and Cook, P. F. (2000) Pyridine nucleotide-dependent $\beta$-hydroxyacid oxidative decarboxylases: An overview. *Protein Pept. Lett. 7*, 281–286.
34. Imada, K., Inagaki, K., Matsunami, H., Kawaguchi, H., Tanaka, H., Tanaka, N., and Namba, K. (1998) Structure of 3-isopropylmalate dehydrogenase in complex with 3-isopropylmalate at 2.0 angstrom resolution: The role of Glu88 in the unique substrate recognition mechanism. *Struct. Folding Des. 6*, 971–982.
35. Miyazaki, J., Asada, K., Fushinobu, S., Kuzuyama, T., and Nishiyama, M. (2005) Crystal structure of tetrameric homoisocitrate dehydrogenase from an extreme thermophile *Thermus thermophilus*: Involvement of hydrophobic dimer-dimer interaction in extremely high thermotolerance. *J. Bacteriol. 187*, 6779–6788.
36. Coleman, D. E., Rao, G. S. J., Goldsmith, E. J., Cook, P. F., and Harris, B. G. (2002) Crystal structure of the malic enzyme from *Ascaris suum* complexed with nicotinamide adenine dinucleotide at 2.3 angstrom resolution. *Biochemistry 41*, 6928–6938.
37. Tao, X., Yang, Z. R., and Tong, L. (2003) Crystal structures of substrate complexes of malic enzyme and insights into the catalytic mechanism. *Structure 11*, 1141–1150.
38. Yang, Z. R., Zhang, H. L., Hung, H. C., Kuo, C. C., Tsai, L. C., Yuan, H. S., Chou, W. Y., Chang, G. G., and Tong, L. (2002) Structural studies of the pigeon cytosolic $NADP^+$-dependent malic enzyme. *Protein Sci. 11*, 332–341.
39. Thompson, J. D., Higgins, D. G., and Gibson, T. J. (1994) CLUSTAL W: Improving the sensitivity of progressive multiple sequence alignment through sequence weighting, position-specific gap penalties and weight matrix choice. *Nucleic Acids Res. 22*, 4673–4680.
40. Lin, Y., Volkman, J., Nicholas, K. M., Yamamoto, T., Eguchi, T., Nimmo, S. L., West, A. H., and Cook, P. F. (2008) Chemical mechanism of homoisocitrate dehydrogenase from *Saccharomyces cerevisiae*. *Biochemistry 47*, 4169–4180.
41. Xu, Y. W., Bhargava, G., Wu, H., Loeber, G., and Tong, L. (1999) Crystal structure of human mitochondrial $NAD(P)^+$-dependent malic enzyme: A new class of oxidative decarboxylases. *Struct. Folding Des. 7*, 877–889.
42. Kiick, D. M., Harris, B. G., and Cook, P. F. (1986) Protonation mechanism and location of rate-determining steps for the *Ascaris suum* nicotinamide adenine-dinucleotide malic enzyme reaction from isotope effects and pH studies. *Biochemistry 25*, 227–236.
43. Park, S. H., Harris, B. G., and Cook, P. F. (1986) pH-dependence of kinetic parameters for oxalacetate decarboxylation and pyruvate reduction reactions catalyzed by malic enzyme. *Biochemistry 25*, 3752–3759.
44. Schimerlik, M. I., and Cleland, W. W. (1977) pH variation of kinetic parameters and catalytic mechanism of malic enzyme. *Biochemistry 16*, 576–583.
45. Weiss, P. M., Gavva, S. R., Harris, B. G., Urbauer, J. L., Cleland, W. W., and Cook, P. F. (1991) Multiple isotope effects with alternative dinucleotide substrates as a probe of the malic enzyme reaction. *Biochemistry 30*, 5755–5763.
46. Gavva, S. R., Harris, B. G., Weiss, P. M., and Cook, P. F. (1991) Modification of a thiol at the active site of the *Ascaris suum* NAD-malic enzyme results in changes in the rate-determining steps for oxidative decarboxylation of L-malate. *Biochemistry 30*, 5764–5769.
47. Karsten, W. E., and Cook, P. F. (1994) Stepwise versus concerted oxidative decarboxylation catalyzed by malic enzyme: A reinvestigation. *Biochemistry 33*, 2096–2103.
48. Karsten, W. E., Lai, C. J., and Cook, P. F. (1995) Inverse solvent isotope effects in the NAD-malic enzyme reaction are the result of the viscosity difference between $D_2O$ and $H_2O$: Implications for solvent isotope effect studies. *J. Am. Chem. Soc. 117*, 5914–5918.
49. Karsten, W. E., Hwang, C. C., and Cook, P. F. (1999) $\alpha$-Secondary tritium kinetic isotope effects indicate hydrogen tunneling and coupled motion occur in the oxidation of L-malate by NAD-malic enzyme. *Biochemistry 38*, 4398–4402.
50. Edens, W. A., Urbauer, J. L., and Cleland, W. W. (1997) Determination of the chemical mechanism of malic enzyme by isotope effects. *Biochemistry 36*, 1141–1147.
51. Schimerlik, M. I., and Cleland, W. W. (1975) Deuterium isotope effects and substrate-specificity of malic enzyme. *Fed. Proc. 34*, 495.
52. Rao, G. S. J., Coleman, D. E., Karsten, W. E., Cook, P. F., and Harris, B. G. (2003) Crystallographic studies on *Ascaris suum* NAD-malic enzyme bound to reduced cofactor and identification of an effector site. *J. Biol. Chem. 278*, 38051–38058.
53. Yang, Z. R., Floyd, D. L., Loeber, G., and Tong, L. (2000) Structure of a closed form of human malic enzyme and implications for catalytic mechanism. *Nat. Struct. Biol. 7*, 251–257.
54. Chang, G. G., and Tong, L. (2003) Structure and function of malic enzymes, a new class of oxidative decarboxylases. *Biochemistry 42*, 12721–12733.
55. Karsten, W. E., Chooback, L., Liu, D., Hwang, C. C., Lynch, C., and Cook, P. F. (1999) Mapping the active site topography of the NAD-malic enzyme via alanine-scanning site-directed mutagenesis. *Biochemistry 38*, 10527–10532.
56. Liu, D., Karsten, W. E., and Cook, P. F. (2000) Lysine 199 is the general acid in the NAD-malic enzyme reaction. *Biochemistry 39*, 11955–11960.
57. Grissom, C. B., and Cleland, W. W. (1988) Isotope effect studies of chicken liver NADP malic enzyme: Role of the metal-ion and viscosity dependence. *Biochemistry 27*, 2927–2934.
58. Rajapaksa, R., Abu-Soud, H., Raushel, F. M., Harris, B. H., and Cook, P. F. (1993) Pre-steady state kinetics reveal a slow isomerization of the enzyme-NAD complex in the NAD-malic enzyme reaction. *Biochemistry 32*, 1928–1934.
59. Berdis, A. J., and Cook, P. F. (1993) Chemical mechanism of 6-phosphogluconate dehydrogenase from *Torula*. *Biochemistry 32*, 2041–2046.
60. Price, N. E., and Cook, P. F. (1996) Kinetic and chemical mechanisms of the 6-phosphogluconate dehydrogenase from sheep liver. *Arch. Biochem. Biophys. 336*, 215–223.
61. Cervellati, C., Dallocchio, F., Bergamini, C. M., and Cook, P. F. (2005) Role of methionine-13 in the catalytic mechanism of 6-phosphogluconate dehydrogenase from sheep liver. *Biochemistry 44*, 2432–2440.
62. Huang, Y. C., and Colman, R. F. (2005) Location of the coenzyme binding site in the porcine mitochondrial NADP-dependent isocitrate dehydrogenase. *J. Biol. Chem. 280*, 30349–30353.
63. Imada, K., Tamura, T., Takenaka, R., Kobayashi, I., Namba, K., and Inagaki, K. (2008) Structure and quantum chemical analysis of $NAD^+$-dependent isocitrate dehydrogenase: Hydride transfer and co-factor specificity. *Proteins 70*, 63–71.
64. Kim, T. K., Lee, P., and Colman, R. F. (2003) Critical role of Lys(212) and Tyr(140) in porcine NADP-dependent isocitrate dehydrogenase. *J. Biol. Chem. 278*, 49323–49331.
65. Lee, P., and Colman, R. F. (2006) Thr(373), Asp(375), and Lys(260) are in the coenzyme site of porcine NADP-dependent isocitrate dehydrogenase. *Arch. Biochem. Biophys. 450*, 183–190.
66. Bzymek, K. P., and Colman, R. F. (2007) Role of $\alpha$-Asp(181), $\beta$-Asp(192), and $\gamma$-Asp(190) in the distinctive subunits of human NAD-specific isocitrate dehydrogenase. *Biochemistry 46*, 5391–5397.
67. Auld, D. S., and Vallee, B. L. (1970) Kinetics of carboxypeptidase-A pH dependence of tripeptide hydrolysis catalyzed by zinc, cobalt, and manganese enzymes. *Biochemistry 9*, 4352–4355.
68. Smith, R. M., and Martell, A. E. (1976) *Critical Stability Constants, Volume 4: Inorganic complexes*, Plenum Press, New York.
69. Miyazaki, K., and Oshima, T. (1993) Tyr-139 in *Thermus thermophilus* 3-isopropylmalate dehydrogenase is involved in catalytic function. *FEBS Lett. 332*, 37–38.

BI8022976